Received: 25 April 2020 | Revised: 14 December 2020 | Accepted: 5 January 2021

DOI: 10.1111/geb.13268

RESEARCH PAPER

Global Ecology and Biogeography | A Journal of Macroecology | WILEY

Macroecological patterns of forest structure and allometric scaling in mangrove forests

Andre S. Rovai[1,2] | Robert R. Twilley[1] | Edward Castañeda-Moya[3] | Stephen R. Midway[1] | Daniel A. Friess[4] | Carl C. Trettin[5] | Jacob J. Bukoski[6] | Atticus E.L. Stovall[7] | Paulo R. Pagliosa[2] | Alessandra L. Fonseca[2] | Richard A. Mackenzie[8] | Aslan Aslan[9] | Sigit D. Sasmito[10,11] | Mériadec Sillanpää[4,12] | Thomas G. Cole[13] | Joko Purbopuspito[14] | Matthew W. Warren[15] | Daniel Murdiyarso[11,16] | Wolfram Mofu[17] | Sahadev Sharma[18] | Pham Hong Tinh[19] | Pablo Riul[20]

[1]Department of Oceanography and Coastal Sciences, College of the Coast & Environment, Louisiana State University, Baton Rouge, LA, USA

[2]Departamento de Oceanografia, Universidade Federal de Santa Catarina, Florianópolis, Brazil

[3]Institute of Environment (OE 148), Florida International University, Miami, FL, USA

[4]Department of Geography, National University of Singapore, Singapore

[5]USDA Forest Service Southern Research Station, Cordesville, SC, USA

[6]Department of Environmental Science, Policy and Management, University of California, Berkeley, Berkeley, CA, USA

[7]NASA Goddard Space Flight Center, Greenbelt, MD, USA

[8]Institute of Pacific Islands Forestry, Pacific Southwest Research Station, USDA Forest Service, Hilo, HI, USA

[9]Southeast Asian Regional Centre for Tropical Biology (SEAMEO BIOTROP), Bogor, Indonesia

[10]Research Institute for the Environment and Livelihoods (RIEL), Charles Darwin University, Casuarina, Northern Territory, Australia

[11]Center for International Forestry Research (CIFOR), Bogor, Indonesia

[12]Research Department, Green Forest Product and Tech. Pte. Ltd., Singapore, Singapore

[13]Department of Natural Resources and Environmental Management, University of Hawai'i at Mānoa, Honolulu, HI, USA

[14]Soil Science Department, Faculty of Agriculture, Sam Ratulangi University, Kampus Kleak-Bahu, Manado, Indonesia

[15]Earth Innovation Institute, San Francisco, CA, USA

[16]Department of Geophysics and Meteorology, Institut Pertanian Bogor, Bogor, Indonesia

[17]Faculty of Forestry, University of Papua, Manokwari, Indonesia

[18]Institute of Ocean and Earth Sciences, University of Malaya, Kuala Lumpur, Malaysia

[19]Faculty of Environment, Hanoi University of Natural Resources and Environment, Hanoi, Viet Nam

[20]Departamento de Sistemática e Ecologia, Centro de Ciências Exatas e da Natureza, Universidade Federal da Paraíba, João Pessoa, Paraíba, Brazil

Correspondence
Andre S. Rovai, Department of Oceanography and Coastal Sciences, College of the Coast & Environment, Louisiana State University, Baton Rouge, LA 70803, USA.
Email: asrovai@gmail.com, arovai1@lsu.edu

Funding information
U.S. Forest Service International Programs; USAID Indonesia Forest and Climate Supports, Grant/Award Number: AG-3187-C-13-0010; NSF, Florida Coastal Everglades Long-Term Ecological Research Program, Grant/Award Number: DEB-1832229; CAPES/CNPq, Grant/Award Number: BEX1930/13-3, BEX18379/12-5

Abstract

Aim: Mangrove wetlands span broad geographical gradients, resulting in functionally diverse tree communities. We asked whether latitudinal variation, allometric scaling relationships and species composition influence mangrove forest structure and biomass allocation across biogeographical regions and distinct coastal morphologies.

Location: Global.

Time period: Present.

Major taxa studied: Mangrove ecosystems.

Methods: We built the largest field-based dataset on mangrove forest structure and biomass to date (*c.* 2,800 plots from 67 countries) to address macroecological

and BEX209666/13-7; Louisiana Sea Grant College

Editor: Andrew Kerkhoff

questions pertaining to structural and functional diversity of mangroves spanning biogeographical and coastal morphology gradients. We used frequentist inference statistics and machine learning models to determine environmental drivers that control biomass allocation within and across mangrove communities globally.

Results: Allometric scaling relationships and forest structural complexity were consistent across biogeographical and coastal morphology gradients, suggesting that mangrove biomass is controlled by regional forcings rather than by latitude or species composition. For instance, nearly 40% of the global variation in biomass was explained by regional climate and hydroperiod, revealing nonlinear thresholds that control biomass accumulation across broad geographical gradients. Furthermore, we found that ecosystem-level carbon stocks (average 401 ± 48 MgC/ha, covering biomass and the top 1 m of soil) varied little across diverse coastal morphologies, reflecting regional bottom-up geomorphic controls that shape global patterns in mangrove biomass apportioning.

Main conclusions: Our findings reconcile views of wetland and terrestrial forest macroecology. Similarities in stand structural complexity and cross-site size–density relationships across multiscale environmental gradients show that resource allocation in mangrove ecosystems is independent of tree size and invariant to species composition or latitude. Mangroves follow a universal fractal-based scaling relationship that describes biomass allocation for several other terrestrial tree-dominated communities. Understanding how mangroves adhere to these universal allometric rules can improve our ability to account for biomass apportioning and carbon stocks in response to broad geographical gradients.

KEYWORDS

aboveground biomass, allometric scaling relationships, biogeography, blue carbon, coastal environmental setting, ecosystem-level carbon, forest structure

1 | INTRODUCTION

Globally, mangroves span two major biogeographical regions, the Indo-West Pacific (IWP) and the Atlantic East Pacific (AEP) (Duke et al., 2017), where they colonize diverse coastal morphologies (Twilley et al., 2018). One of the most distinctive evolutionary outcomes between IWP and AEP regions is the number of mangrove species; the IWP region contains 54 mangrove species, whereas the AEP has 17 species, including mangrove associates (Duke et al., 2017). This east–west gradient in species diversity, in addition to latitudinal range, has always intrigued coastal wetland scientists with regard to whether these biogeographical regions can explain the epicentre of mangrove genetic diversity and distribution (Ellison, 2002). However, the influence of regional species diversity gradients on mangrove ecosystem attributes such as carbon storage is limited in terms of number and geographical distribution of sites that have been assessed globally (Atwood et al., 2017; Kauffman et al., 2020). Moreover, morphological variations in plant traits, both within and across these regions (Duke et al., 2017), raise the question of whether the diversity in tree life-forms between IWP and AEP species could reduce the accuracy of universal models that estimate aboveground biomass (AGB) across these broad biogeographical regions.

In addition to biogeographical-scale processes, coastal morphology has been shown to be important in shaping the global geographical variability of the ecological attributes of mangroves from regional patterns (Woodroffe et al., 2016). Diverse coastal morphologies (or environmental settings) include river-, tide- and wave-dominated, carbonate and arheic systems (Dürr et al., 2011). These coastal environmental settings are shaped by geophysical (e.g., tidal amplitude, river discharge, wave energy) and climatic (e.g., temperature, precipitation, evapotranspiration) factors (Twilley et al., 2018). Altogether, these coastal forcings produce conspicuous soil nutrient [nitrogen (N) and phosphorus (P)] stoichiometric patterns among distinct coastal environmental settings (Rovai et al., 2018), to which mangrove plants respond by shifting carbon allocation between above- (shoot) and belowground (root) compartments (Castañeda-Moya et al., 2013; Cormier et al., 2015).

We investigated how biogeography and coastal morphology influence global mangrove forest structural attributes (e.g., basal area,

tree density) and biomass. In particular, we examined plot-level forest allometric scaling relationships between IWP and AEP mangroves and among distinct coastal morphologies, and whether these traits can influence model-based generalizations of forest structure and carbon stocks across these regions. Also, we asked whether species richness is an important trait to determine forest structure and carbon stocks in mangrove AGB. We hypothesized that forest allometric scaling relationships are invariant to latitudinal range (Enquist & Niklas, 2001) despite evolutionary life history between IWP and AEP mangroves and its outcomes (e.g., eastward species biodiversity gradient). Furthermore, considering that resource allocation per unit area in tree-dominated communities is independent of individual tree size or species composition (Enquist et al., 1998), we hypothesized that forest structural complexity (*sensu* Holdridge et al., 1971) and cross-site size–density relationships (White et al., 2007) in mangroves are similar across biogeographical regions and coastal morphologies. We also tested whether regional drivers of coastal morphology, such as geophysical (tidal range and riverine input) and climatic (temperature, precipitation and evapotranspiration) variables, control forest structure and carbon storage in mangrove AGB globally. In this regard, we posited that mangrove AGB increases with inorganic suspended matter (a proxy for riverine nutrient input), tidal amplitude and the duration of inundation, temperature and precipitation, and decreases with potential evapotranspiration. Finally, we tested whether tropical cyclone frequency is a significant driver of mangrove AGB variability globally, as has been suggested recently (Simard et al., 2019).

To answer these questions, we collated data from studies distributed across 64% of the nations that contain mangroves, significantly expanding prior compilations (Hutchison et al., 2014; Kauffman et al., 2020; Simard et al., 2019; Twilley et al., 1992; for a comparison among studies, see Table 1; Supporting Information Figure S1), and draw on this new dataset (Figure 1; Supporting Information Table S1) to test how geographical gradients drive mangrove forest structure and AGB density globally. Lastly, we integrated our AGB predictions with existing estimates of soil organic carbon (SOC) from a range of sources in addition to a multiplier to account for belowground biomass (BGB) to derive ecosystem-level (biomass plus SOC) carbon stocks globally.

2 | METHODS

2.1 | Data acquisition and handling

We compiled published and unpublished studies (including theses, dissertations and reports) totalling 493 sources from 67 countries reporting on nearly 2,800 plots world-wide that contained mangrove forest structural attributes (stand basal area and density, diameter, mean canopy height and species composition) and aboveground biomass data (Figure 1; see also Supporting Information and Table S1 therein). Field plots were classified by the major biogeographical region to which they belong (AEP or IWP). We also classified sites according to coastal morphology under the following categories: river-dominated [large rivers (I) and small deltas (II)], tidal systems [estuaries, rias (III)] lagoons [sand bar estuaries and composite river/wave-dominated (IV)], peat-dominated [carbonate (V)] and arid [arheic (VI)] coastlines (for details, see Dürr et al., 2011; Twilley et al., 2018; Figure 1a–g; Supporting Information Table S1).

2.2 | Statistical analyses and geospatial modelling

We used Kruskal–Wallis and pairwise Wilcoxon rank sum tests to assess differences ($p < .05$) in mangrove forest structure, complexity and AGB between biogeographical regions and among distinct coastal environmental settings, in addition to linear and nonlinear regression to assess allometric scaling relationships. Forest structural complexity was assessed using Holdridge's complexity index (Holdridge et al., 1971), which is the product of mean canopy height, stand basal area, stand density and the number of species (for details, see additional text provided as Supporting Information).

For the geospatial modelling of AGB, we constrained our predictions to a global mangrove coverage area of *c.* 81,800 km^2 (Hamilton & Casey, 2016) but resampled to a .1° × .1° cell resolution (approximately 10 km × 10 km at the equator) in order to bring all gridded environmental compilations to a consistent resolution (see Supporting Information Table S2). We computed 75th percentile values for each .1° × .1° cell containing plot-level AGB observations (a total of 2,739 plots; for details on plot exclusion criteria, see Supporting Information). This data-aggregation procedure produced 524 .1° × .1° cells with AGB values, which is the sample size we used in our geospatial modelling analysis.

Based on the literature (Hutchison et al., 2014; Osland et al., 2017; Rovai et al., 2016; Schaeffer-Novelli et al., 1990; Simard et al., 2019; Twilley et al., 1992; Woodroffe et al., 2016), we initially identified 13 variables available globally as gridded data that are suggested to influence mangrove AGB. These variables included derivatives of climatic factors [e.g., minimum temperature, minimum precipitation, mean annual potential evapotranspiration (PET), PET from the driest, wettest, warmest and coldest quarters, frequency of tropical cyclones] and geophysical variables, such as tidal frequency, amplitude and duration, and inorganic and total suspended matter, as a proxy to riverine sediment and nutrient load (for details, see Supporting Information Table S2). We then extracted these environmental correlates for each .1° × .1° cell containing an AGB value. Environmental variables with autocorrelation ($\rho > .6$) or collinearity problems (variance inflation factor > 3) were removed from further analysis (Supporting Information Figure S2; Table S3).

To determine the potential for improvements in spatial predictions stemming from different modelling approaches, we developed and compared the outputs of models based on random forest machine learning (RF) and multiple linear regression (MLR).

TABLE 1 Cross-study comparison showing number of sites (or cells) and plots, methods and predictors used to estimate global mangrove biomass

Mean AGB (Mg/ha)	Mangrove area used (km^2)	Global AGB (PgC)	Global BGB (PgC)	Global AGB (PgC) normalized to 81,849 km^2[a]	Method used to estimate global AGB	Number of sites used to model/estimate AGB	Environmental predictors used to model AGB	Source
164; 128[b]	81,849 Hamilton and Casey (2016), mangrove area for 2012	.81; .63[b]	.40; .31[b]	.81; .63[b]	Bioclimatic–geophysical model, random forest machine learning, multiple linear regression	$n = 524$ .1° × .1° cells (2,739 plots from 67 countries)	(a) Minimum temperature of coldest month; (b) precipitation of driest month; (c) potential evapotranspiration of driest quarter; (d) annual average tidal cycle amplitude; and (e) annual average duration of tidal cycles	This study
239	137,600 Giri et al. (2011)	1.6	–	.95	Mean AGB reference value multiplied by mangrove area cover	$n = 190$ sites (*c.* 1,000 subplots from 15 countries)	NA	Kauffman et al. (2020)
129	137,600 Giri et al. (2011)	.78	.38	.46	Allometric equations (AGB estimated from tree height) using remotely sensed tree heights	$n = 14$ sites (332 plots from 10 countries)	NA	Simard et al. (2019)
	83,495 Hamilton and Casey (2016), mangrove area for 2000	.82	.41	.80	Estimates based on models by Hutchison et al. (2014), Twilley et al. (1992)	NA	NA	Hamilton and Friess (2018)
146	130,420	.9	.34	.56	Allometric equations (AGB estimated from tree height) using remotely sensed tree heights	NA	NA	Tang et al. (2018)
185	153,141 Spalding et al. (2010)	1.34	.53	.72	Bioclimatic model, multiple linear regression	$n = 52$ .1° × .1° cells (102 plots from 19 countries)	(a) Mean temperature of warmest quarter; (b) mean temperature of coldest quarter; (c) precipitation of wettest quarter; and (d) precipitation of driest quarter	Hutchison et al. (2014)
178	240,000 WRI/IIED (1986)	2.34	1.69	.80	Latitude-based model, linear regression	$n = 35$ sites from 11 countries	Latitude	Twilley et al. (1992)

Note: See Figure S1 for spatial distribution of datasets used in each study.

Abbreviations: AGB, aboveground biomass; BGB, belowground biomass; NA, not applicable.

[a]Mangrove area for 2012 from Hamilton and Casey (2016).

[b]Estimates after semicolon were produced using the multiple linear regression approach (for details, see additional text provided as Supporting Information).

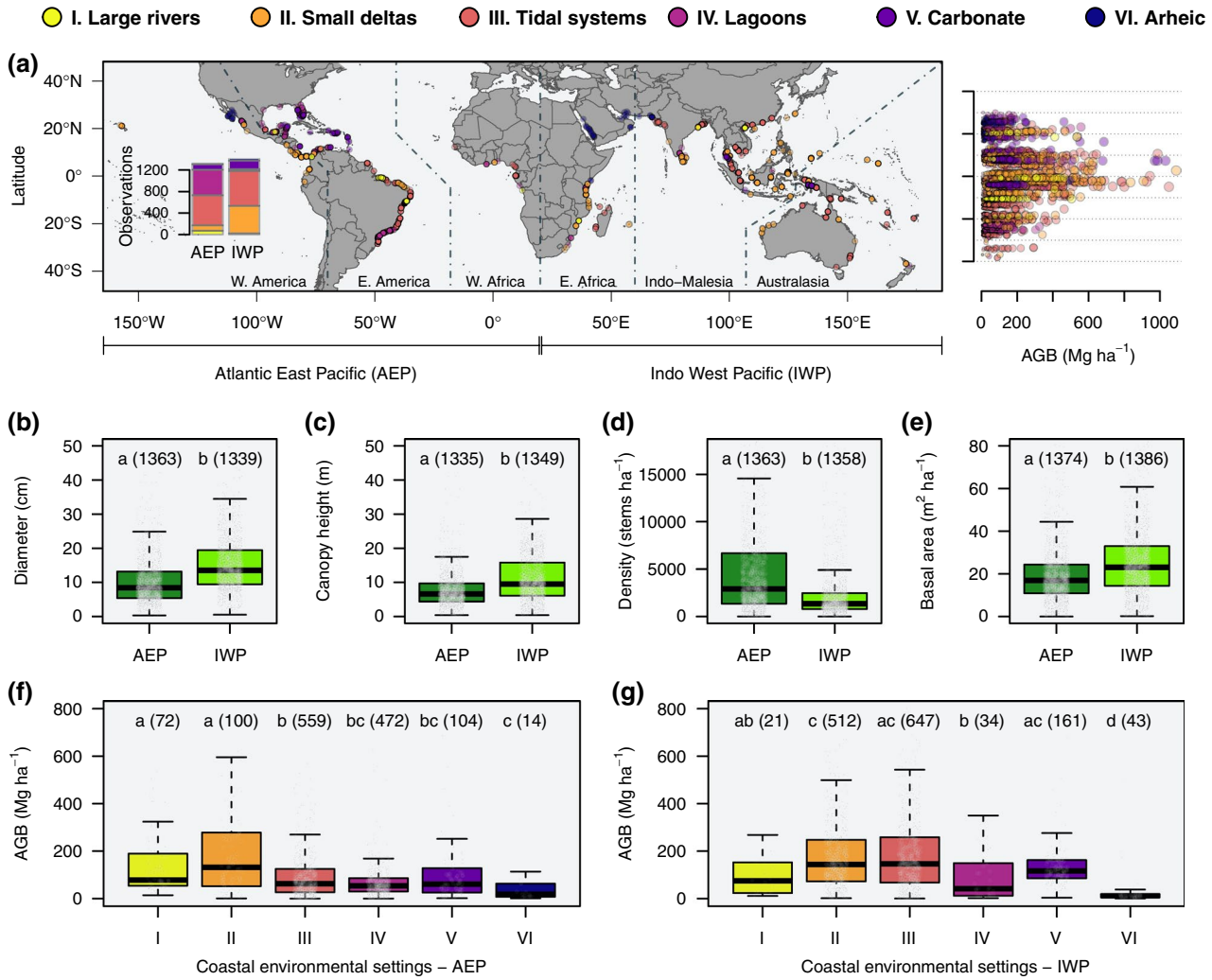

FIGURE 1 Distribution of mangrove forest structural attributes and aboveground biomass (AGB) across biogeographical regions, latitude and coastal environmental settings. (a) The total number of observations for AGB is distributed evenly between Atlantic East Pacific (AEP) and Indo-West Pacific (IWP) biogeographical regions but varies across distinct coastal environmental settings. The highest AGB values are generally found in the low tropics, but tall, well-developed stands also occur near subtropical zones. (b–e) Tree diameter, height and basal area are higher in IWP mangroves, but density (shown only up to 18,000 stems/ha to enhance visualization, but for the full range, see Supporting Information Table S1) is higher in AEP. Different lowercase letters on top of groups and numbers within brackets denote the statistical difference ($p < .05$) and number of observations for each group, respectively. (f,g) Mangrove AGB decreases: (f) from river-dominated to carbonate and arheic coastlines in the AEP, and (g) from river- and tide-dominated to arheic coastal environmental settings in the IWP [Colour figure can be viewed at wileyonlinelibrary.com]

For RF models, we compared the performance of a model using all variables (including those found to show collinearity; Supporting Information Figure S2) with a reduced model (excluding collinear variables). The prediction error of the model was assessed with leave-one-out cross-validation (Liaw & Wiener, 2002). The marginal effect of environmental drivers on mangrove AGB predictions was examined further using partial dependence plots. For MLR models, data were cube root transformed to meet normality assumptions (Supporting Information Figure S3). The Akaike information criterion and ANOVA were used to select the model that best described our dataset (Supporting Information Table S4). The relative importance of predictors was assessed using R^2 partitioning (for details, see the Supporting Information). As for RF, we assessed the performance of the model using leave-one-out cross-validation. The RF and MLR modelling were completed in R using the *randomForest* and *raster* packages (Hijmans, 2020; Liaw & Wiener, 2002; R Core Team, 2020).

2.3 | Computing global ecosystem-level carbon stocks in mangroves

We estimated global mangrove ecosystem-level carbon stocks by coupling the AGB map we produced with published estimates of the top 1 m SOC (Rovai et al., 2018). Global BGB estimates were derived from AGB using a BGB:AGB ratio of .5 (Hamilton & Friess, 2018; for details, see also Supporting Information Figure S4). To calculate carbon stocks in both AGB and BGB where data were not already reported in

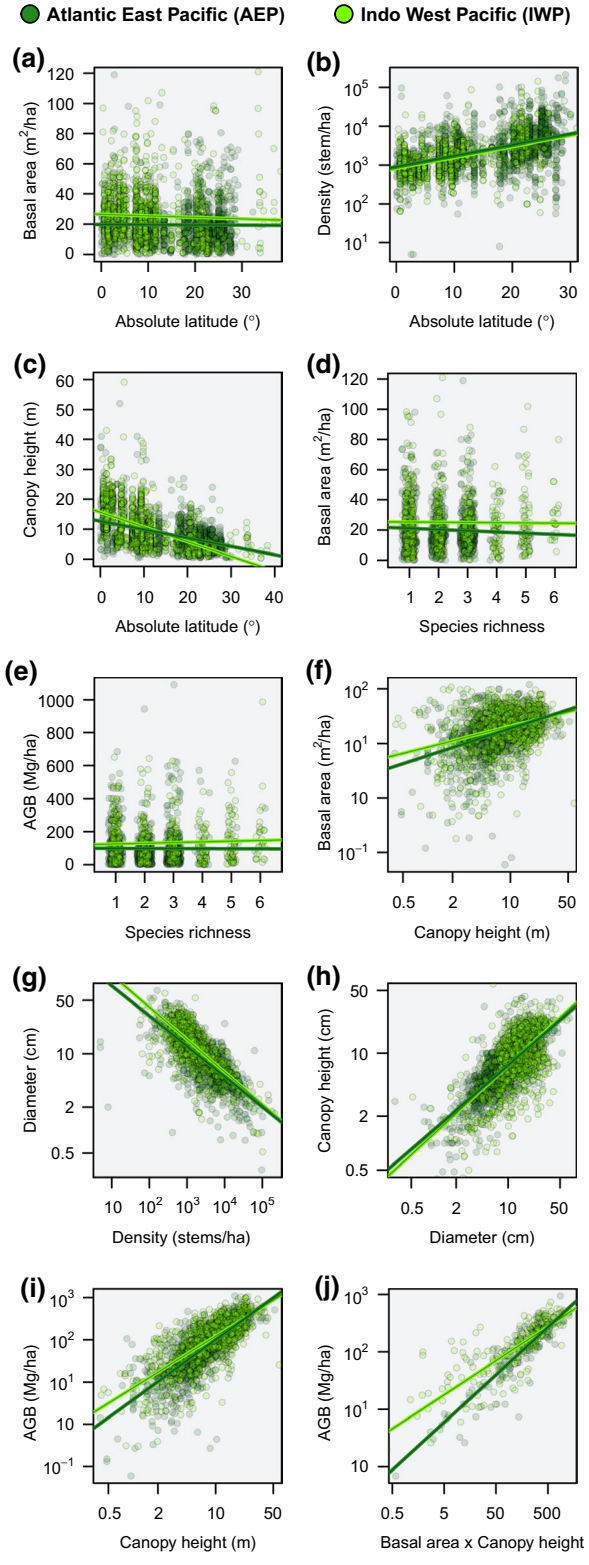

FIGURE 2 Relationships between mangrove forest structural attributes and: (a–e) latitude or species richness, and (f–j) allometric scaling relationships (log-scale) for Atlantic East Pacific and Indo-West Pacific mangroves. (a) Basal area did not vary with latitude, whereas (b) stem density (*y* axis in log-scale owing to large range) increased with latitude. (c) Mean canopy height decreased with latitude. (d,e) Basal area and aboveground biomass (AGB) did not vary with species richness (a regression was fitted to all data, but only sites with up to six species are shown to improve visualization). (f) Basal area and mean canopy height were weakly correlated. (g) Tree diameter decreases with increasing stem density. (h) Mean canopy height is positively correlated with diameter. (i,j) AGB is positively correlated with (i) mean canopy height, and with (j) the volumetric product of stand basal area and canopy height. Transparency was added to symbols to improve visualization of overlapping values [Colour figure can be viewed at wileyonlinelibrary.com]

carbon units, we used a conversion factor of .475, which is consistent with a previous global synthesis on mangrove carbon stocks (Hamilton & Friess, 2018). Finally, we used a global coastal geomorphology classification system (Dürr et al., 2011; Twilley et al., 2018) to classify ecosystem-level carbon stock for each type of coastal environmental setting where mangroves occur. All statistical and geospatial analyses described in the items above were conducted in R (R Core Team, 2020).

3 | RESULTS

3.1 | Influence of latitude, biogeography and species richness on mangrove forest structure, allometry and AGB

Latitude explained only *c*. 10% of the global variability in mangrove AGB (R^2 = .09, p < .001 for AEP; R^2 = .11, p < .001 for IWP; Figure 1a). Mangrove forest structural attributes differed between AEP and IWP biogeographical regions (Figure 1b–e). Mean (± 1 *SE*) diameter, tree height and basal area were significantly higher in the IWP region (15.29 ± .22 cm, 11.12 ± .19 m and 25.18 ± .45 m^2/ha, respectively) than in AEP mangroves (10.31 ± .21 cm, 7.84 ± .15 m and 19.37 ± .38 m^2/ha, respectively), whereas tree density was higher in AEP (6,756 ± 399 stems/ha) than in IWP (3,126 ± 325 stems/ha).

Similar to AGB, basal area also did not vary with latitude (p = .75 and p = .11 for AEP and IWP, respectively; Figure 2a), whereas stem density increased with latitude (R^2 = .17, p < .001 for AEP, and R^2 = .22, p < .001 for IWP; Figure 2b). Canopy height decreased with latitude (R^2 = .17, p < .001 for AEP, and R^2 = .28, p < .001 for IWP; Figure 2c). Neither basal area nor AGB was significantly related to species richness (p > .05; Figure 2d,e).

Allometric scaling relationships were nearly identical between biogeographical regions (Figure 2f–j). Basal area and mean canopy height were weakly correlated (R^2 = .15, p < .001 for AEP, and R^2 = .11, p < .001 for IWP; Figure 2f). Density–diameter relationships were indistinguishable between AEP and IWP mangroves (R^2 = .55, p < .001 for AEP, and R^2 = .51, p < .001 for IWP; Figure 2g). Mean canopy height and diameter were positively correlated for both AEP (R^2 = .60, p < .001) and IWP (R^2 = .38, p < .001) (Figure 2h). Mean canopy height explained 56% and 57% (p < .001 for both relationships) of AGB variability in the AEP and IWP regions, respectively (Figure 2i), suggesting that other stand mangrove stocking attributes (e.g., basal area) influence the allocation of AGB across broad geographical gradients (Bukoski et al., 2020). Combining basal area with canopy height significantly improved AGB predictions in both regions (R^2 = .81, p < .001 for AEP, and R^2 = .65, p < .001 for IWP; Figure 2j).

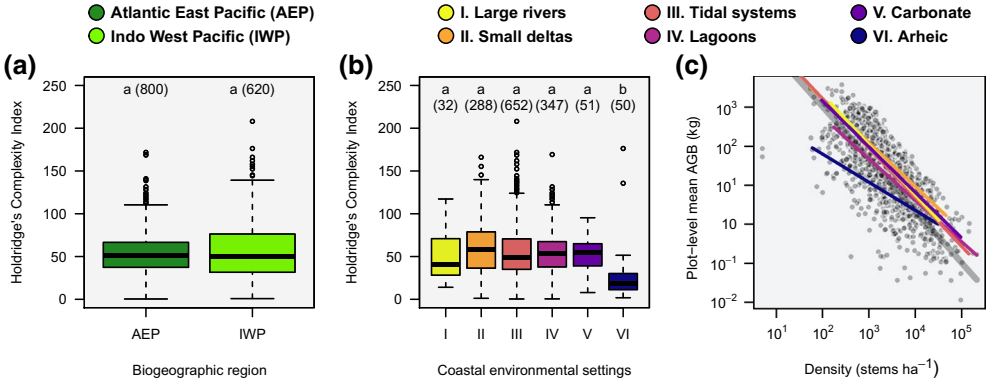

FIGURE 3 Variability of mangrove forest structural complexity index and cross-site size–density relationships across biogeographical regions and coastal environmental settings. (a,b) Complexity indices are similar (a) between biogeographical regions, and (b) among coastal environmental settings, except for arheic systems. (c) Mass–density relationships (in log-scale) across distinct coastal environmental settings follow a fractal-like universal scaling exponent of −4/3, represented here by the continuous black line (for coefficients of models, see Supporting Information Table S5) [Colour figure can be viewed at wileyonlinelibrary.com]

3.2 | Trends in mangrove forest structure and AGB with coastal morphology

Mangrove AGB decreased significantly from river- and tide-dominated systems to arheic coastal environmental settings in both biogeographical regions ($p < .001$; Figure 1f,g). Higher AGB was found in small deltas (type II) in the AEP (185 ± 18 Mg/ha) and in small deltas and tide-dominated coastlines (types II and III, respectively) in the IWP region (180 ± 6 and 188 ± 6 Mg/ha, respectively). In both regions, mangroves located at the mouth of large rivers (type I) had lower AGB than mangroves located in small deltas (type II). Mangrove AGB in carbonate settings (type V) was comparable to tide-dominated systems (98 ± 12 and 92 ± 4 Mg/ha, respectively) in the AEP region and to river- and tide-dominated coastlines in the IWP (147 ± 11, 180 ± 6 and 188 ± 6 Mg/ha, respectively). Mangrove AGB in lagoons (type IV) showed intermediate values (70 ± 3 and 81 ± 15 Mg/ha in AEP and IWP, respectively), relative to river- and tide-dominated and dry coastlines (arheic) AGB estimates in both biogeographical provinces. The lowest AGB was found in arheic coastlines (32 ± 9 and 33 ± 12 Mg/ha in AEP and IWP, respectively).

The structural complexity index of mangrove stands (mean ± 1 *SE*) did not differ between biogeographical regions (52.98 ± .86 for AEP, and 56.64 ± 1.38 for IWP, $p = .65$; Figure 3a) or among most coastal environmental settings ($p > .05$; Figure 3b), except for arheic systems, where the complexity index was significantly lower (26.36 ± 4.22) than other coastal settings combined (55.61 ± .77). Furthermore, cross-site relationships between average tree biomass and stand density were remarkably similar among distinct environmental settings (Figure 3c; Supporting Information Table S5), closely following a universal fractal-like mass–density relationship that explains allocation of resources across several terrestrial tree-dominated communities (Enquist et al., 1998).

3.3 | Global variability and drivers of mangrove AGB

Although both the RF and MLR methods converged on the importance of macroscopic factors that control variation in mangrove AGB globally (for detailed MLR results, see Supporting Information), the RF approach improved spatial predictions, explaining 36% of the global variation in mangrove AGB (Figure 4a). Thus, we opted for using the RF predictions to compute ecosystem-level carbon stock estimates in our further analyses.

Globally, per unit area and total AGB estimates produced with RF were higher than those produced by the MLR model, at 164 ± .36 Mg/ha (range, 15–516 Mg/ha) and 1.71 Pg, respectively (Figure 4a,b; Table 1). On a percentage difference basis, predictions differed mostly from −25 to 75% (5th percentile = −45%; 95th percentile = 130%), and RF predictions were *c.* 29% higher relative to MLR output (Figure 4c). Moreover, the RF algorithm fitted to the same suite of significant ($p > .05$) environmental variables determined by the MLR approach [tidal amplitude (TDamp) and duration (TDdur), potential evapotranspiration of the driest quarter (PETdry), minimum temperature of the coldest month (Tmin) and precipitation of the driest month (Pmin); for details, see Supporting Information] reduced the root mean square error (RMSE) of the model (Figure 4d, blue dots; RMSE = 108 Mg/ha, $R^2 = .36$) relative to the MLR (Figure 4e; RMSE = 121 Mg/ha, $R^2 = .24$). Below 200 Mg/ha AGB, where 76% of our data exist, MLR had less positively biased predictions (MLR = 5.7%; RF = 52.6%), whereas RF performed marginally better above 200 Mg/ha AGB (MLR = −56.7%; RF = −38.7%; Figure 4f). Lastly, although machine learning methods are generally insensitive to autocorrelation and collinearity issues, the RF algorithm minimally improved the reduced the accuracy of the model when fitted to all 13 preselected environmental variables (Figure 4d, cyan dots; RMSE = 106 Mg/ha, $R^2 = .38$; for autocorrelation and multicollinearity tests, see also Supporting Information Figure S2; Tables S2 and S3).

The overall improvement in AGB predictions was attributable, in part, to the fact that the RF method captured nonlinear trends to which the MLR approach is inherently insensitive (Figure 5). Consistent with MLR, RF ranked Pmin, Tmin, PETdry, TDamp and TDdur, in that order, as important variables, with a mean decrease in accuracy of 34, 31, 28, 27 and 24%, respectively. Mangrove AGB increased steadily until Pmin reached 250 mm/month and seemed to level off after this threshold was surpassed (Figure 5a,b). Likewise, AGB was relatively constant at *c.* 110 Mg/ha, increasing sharply nearly twofold when Tmin reached 20°C, after which its

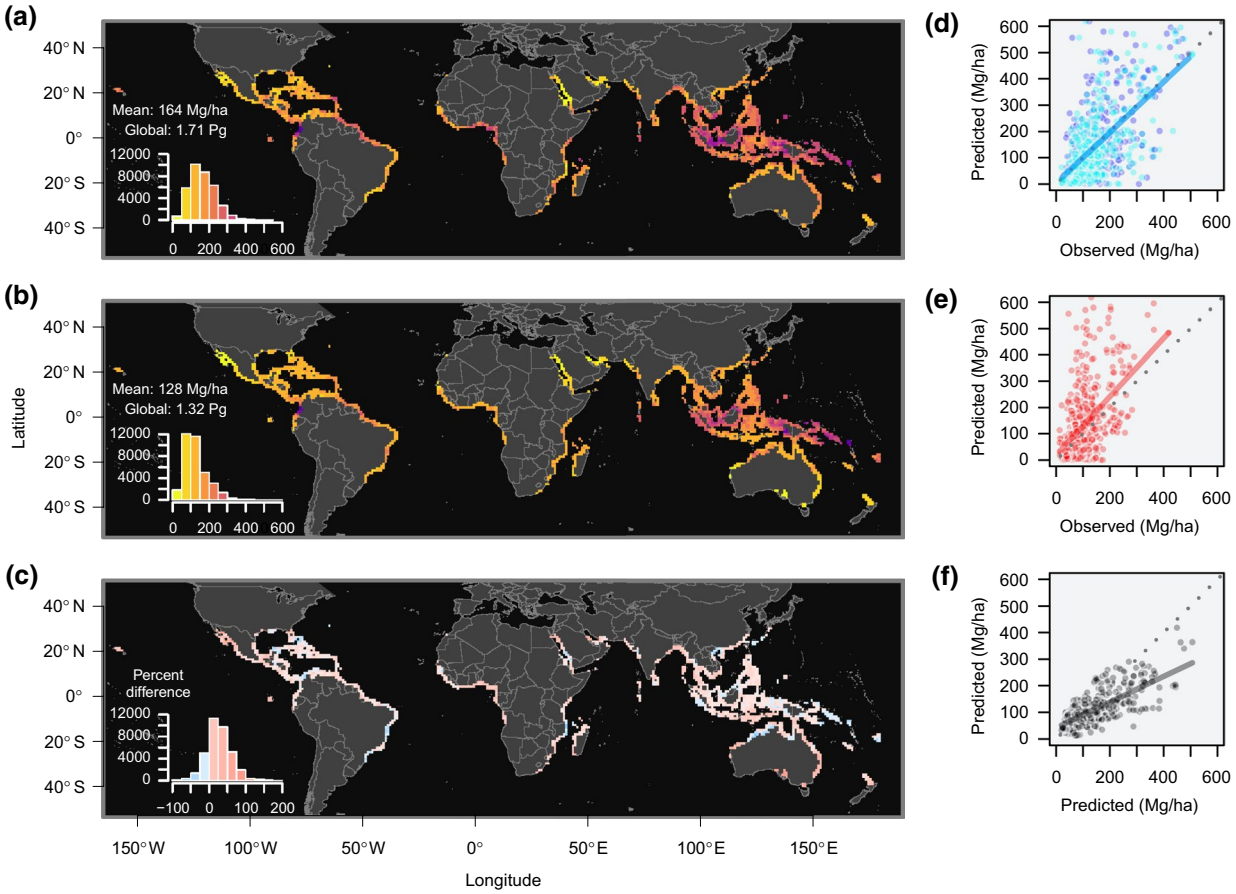

FIGURE 4 Predicted global mangrove aboveground biomass (AGB) and cross-validation plots. (a) Random forest (RF) and (b) multiple linear regression (MLR) approaches fitted to significant environmental variables produced similar mangrove AGB predictions. (c) Percentage differences between modelling approaches varied from −25 to 75%, indicating that RF predictions were, in general, higher relative to MLR output. Histograms show the distribution of predicted AGB values. (d–f) Cross-validation plots show that (d) the RF algorithm fitted to the same suite of significant environmental variables used in the (e) MLR analysis (RMSE = 119 Mg/ha, R^2 = .22) reduced the RMSE of the model (d, blue dots; RMSE = 108 Mg/ha, R^2 = .36). Dotted lines in d–f show the 1:1 relationship. Even when fitted to all 13 preselected environmental variables (see Supporting Information Table S2), the RF algorithm improved the accuracy of the reduced model minimally (d, cyan dots; RMSE = 106 Mg/ha, R^2 = .37). (f) When regressed against one another, MLR (*x* axis) underestimated AGB relative to RF predictions (*y* axis), particularly for higher-AGB plots. Predictions are depicted at 1° × 1° resolution to enhance visualization [Colour figure can be viewed at wileyonlinelibrary.com]

effect on AGB seemed to be less prominent (Figure 5c,d). PETdry overall reduced mangrove AGB (Figure 5e,f). The effects of hydroperiod on mangrove AGB were striking, with AGB increasing sharply from micro- to mesotidal (i.e., tidal range > 2 m) and plateauing after this threshold (Figure 5g,h). Moreover, the global distribution of mangrove AGB appeared to have a unimodal relationship with tidal cycle duration (Figure 5i,j).

3.4 | Global trends in mangrove ecosystem-level carbon stocks

Globally, 2.12 PgC (63%) of carbon stocks were distributed in IWP mangroves and 1.26 PgC in the AEP region. This distribution reflects differences in mangrove area between these regions (IWP = 49,707 km^2 and AEP = 32,070 km^2; Hamilton & Casey, 2016), given that per unit area estimates for IWP and AEP mangroves were similar at 426 and 393 MgC/ha, respectively. Nearly 35% (1.21 PgC) of carbon in mangroves is stored in biomass (0.81 and 0.40 PgC in AGB and BGB, respectively), relative to the top 1 m SOC stocks (2.26 PgC; Rovai et al., 2018). Across coastal morphologies, predicted carbon stocks in biomass decreased from river- and tide-dominated to arheic coastlines (Figure 6a). Combined with SOC (Figure 6b), ecosystem-level carbon stocks varied by < 110 MgC/ha among distinct coastal morphologies (mean, 401 ± 48 MgC/ha; range, 343 ± 78 MgC/ha in arheic to 451 ± 57 MgC/ha in carbonate coastlines; Figure 6c).

4 | DISCUSSION

4.1 | Global patterns of mangrove forest structural development and allometric scaling relationships

Forest structural attributes were higher in IWP mangroves, partly reflecting the distribution of mangrove extent in this region, which

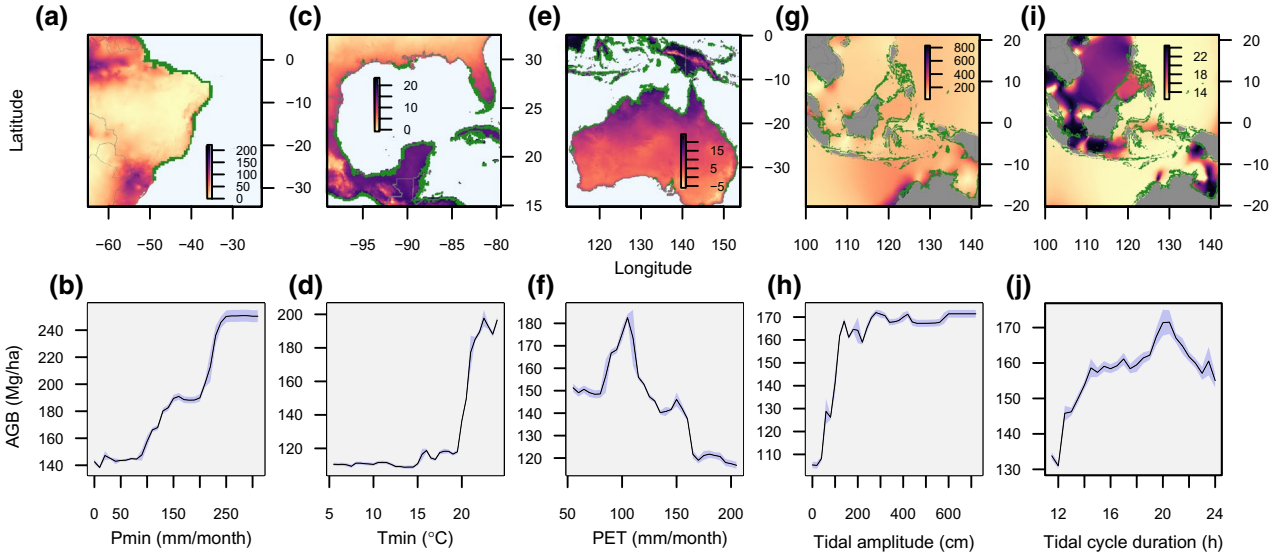

FIGURE 5 Marginal effects of significant global environmental drivers to variation in mangrove aboveground biomass (AGB). Top row, regional subsets are show as an example of how these variables vary over broad geographical gradients: minimum precipitation of driest quarter (Pmin; a,b) along the Brazilian coastline; minimum temperature of coldest month (Tmin; c,d) in the Gulf of Mexico; potential evapotranspiration for the driest quarter (PET; e,f) in part of Oceania; tidal amplitude (g,h) and tidal cycle duration (i,j) along Indonesia and Papua. Mangrove area distribution is shown in dark green. Bottom row, partial dependence plots generated using global random forest predictions suggest nonlinear relationships between mangrove AGB and these environmental drivers. The shaded blue areas along average trend lines show ± 1 *SD* [Colour figure can be viewed at wileyonlinelibrary.com]

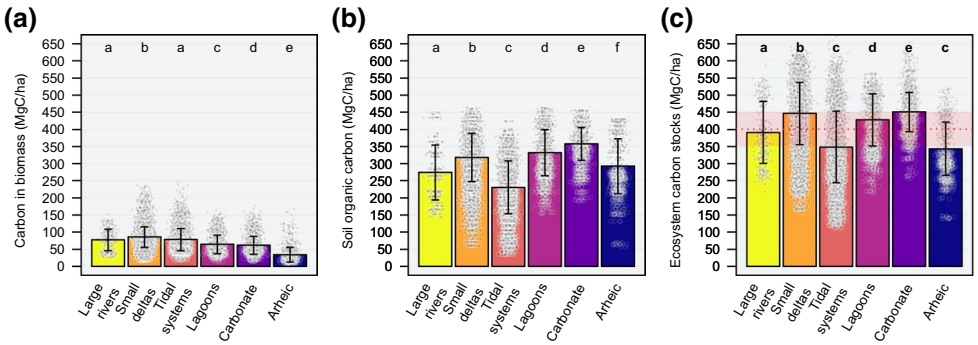

FIGURE 6 Modelled mangrove ecosystem-level carbon stocks across distinct coastal environmental settings. (a) Carbon stored in biomass (above- and belowground combined) decreased from river- and tide-dominated to arheic coastlines, except for carbonate coastal environmental settings, mirroring field-based observations. Bars show the mean (± 1 *SD*) carbon stock values, and different letters above each bar show statistical difference ($p < .05$) among coastal environmental settings, respectively. (b) Top 1 m soil organic carbon (SOC) stocks are lower in river- and tide-dominated coastlines and higher in lagoons and carbonate settings. (c) Site-specific carbon stocks are highly variable across coastal settings, but on a broader scale average similar ecosystem-level (biomass and soil combined) amounts. The shaded red band represents the mean (thick red dotted line) ± 1 *SD* (thin red dotted lines) across all coastal environmental settings [Colour figure can be viewed at wileyonlinelibrary.com]

is concentrated mostly around the equator (i.e., 21,294 km^2 or 26% of the global mangrove area between 5° S and 5° N relative to 13,074 km^2 or 16% of the global mangrove cover for the same latitudinal zone in the AEP). Along the equator, the environmental conditions (e.g., higher precipitation and temperature, lower seasonality) allow for greater mangrove forest structural development (Hutchison et al., 2014; Twilley et al., 1992). In addition, the IWP region has more observations from small deltas and tidal systems, which for both regions showed higher forest structural development (Figure 1a). However, tree allometric scaling relationships suggest that differences in tree physiognomy and species composition between IWP and AEP mangroves are not determining factors for carbon storage in AGB at the scale of our study, in support of the invariant scaling relationships hypothesis (Enquist & Niklas, 2001). Interestingly, basal area did not vary with latitude (Figure 2a), reflecting biomass apportioning through latitude, with the development of denser forest stands with a reduced diameter range towards subtropical zones and well-developed stands with fewer large-diameter trees in lower latitudes (Figure 2b). In contrast, tree height decreased with increasing latitude, indicating that forest stands with

similar canopy heights at any given latitude have highly variable carbon standing stock capacities (Figure 2c,f).

We also examined trends in basal area and AGB in response to species richness between biogeographical regions. The absence of relationship between these structural attributes and the number of species suggests that plant biodiversity has a secondary or even neutral effect on carbon allocation at the ecosystem level. Although the invariance of AGB to species composition has been suggested for mangroves, these assumptions were based on fewer site- and species-specific tree-level allometric relationships (Komiyama et al., 2008). In the present study, we extrapolated the analysis to the global scale using plot-level data that span broader geographical gradients and included much larger numbers of mangrove tree species. This finding is also seen in terrestrial forests, where AGB does not seem to be related positively to species richness in highly diverse, mature tropical forests (Ferreira et al., 2018). Notably, mangrove ecosystems are far less diverse than other tropical and subtropical tree communities. Indeed, despite the overall greater species diversity in the IWP region, the number of species at a site level is similar between biogeographical regions, with 74% and 97% of plots in IWP and AEP containing up to three species, respectively (Supporting Information Figure S5). Therefore, if our results hold with trends demonstrated for other tropical tree communities (Ferreira et al., 2018), the relationship between carbon stocks in mangrove AGB and plant biodiversity might be expectedly weak. Furthermore, our results are in agreement with the allometric scaling theory established for terrestrial forests, where tree density-dependent relationships exert a stronger control on biomass partitioning per unit of forest floor than species composition (Enquist & Niklas, 2001).

Cross-site size–density relationships (White et al., 2007) held consistent between IWP and AEP mangroves, suggesting that mangroves exhibit similar resource partitioning strategies across broad geographical gradients, thus allowing for modelling generalizations about forest structure and biomass apportioning despite distinct biogeographical histories. Our data also showed remarkable similarities in stand structural complexity between biogeographical regions and among most coastal environmental settings (Figure 3a,b), underscoring the concept that AGB allocation in mangrove ecosystems is independent of individual tree size (Enquist et al., 1998). This trend can be explained mainly by cross-site size–density relationships revealed by our data (Figure 3c) and, to a lesser extent, by species composition, considering that plot-level species diversity was similar between AEP and IWP mangroves. These findings provide further support to the concept that mangroves follow closely a fractal-based mass–density scaling relationship for several other terrestrial tree-dominated communities, where tree mass scales with a thinning exponent of −4/3 (Enquist et al., 1998; Enquist & Niklas, 2001). Although within-site self-thinning relationships have been described for mangrove forests elsewhere (Analuddin et al., 2009; Kamara & Kamruzzaman, 2020; Rovai et al., 2021), our results suggest that these allometric rules are consistent across biogeographical and coastal geomorphic spatial scales (e.g., cross-site; White et al., 2007).

However, the structural complexity and tree mass–density relationship of arheic mangroves differed from stands developing in other coastal environmental settings (Figure 3c; Supporting Information Table S5). The change in the slope relative to the fundamental allometric relationship suggests that trees in arheic environments have developed a different biomass allocation strategy in response to stressors (e.g., low precipitation, high evapotranspiration, hypersalinity; for a comprehensive review, see Adame et al., 2020). For example, at 100 stems/ha, three times less biomass can be supported in arheic mangroves relative to other coastal environmental settings (Figure 3c), suggesting that the formation of higher-AGB mangrove stands with sparse individuals is an ecosystem strategy to reduce resource use competition.

4.2 | Global distribution of mangrove AGB in response to coastal environmental settings

Our mangrove AGB data strongly suggest that regional coastal environmental settings exert a bottom-up control by sourcing sediment and nutrient load, resulting in global patterns of mangrove biomass production and partitioning. Higher-AGB stands were generally associated with river- and tide-dominated systems in both biogeographical regions. Interestingly, mangroves located at the mouth of large rivers had lower AGB than in smaller deltas. Although most mangrove species can grow in freshwater, controlled greenhouse experiments have shown that optimal salinity conditions for tree development and biomass growth occur where salinity levels are between 5 and 75% of seawater, with the considerable range being dependent on species (Ball, 2002). Although the physiological requirements to support mangrove biomass growth in saline conditions remain elusive (Krauss & Ball, 2013), it is reasonable to conjecture that where both mangroves and freshwater forested wetlands overlap, production of mangrove biomass is constrained relative to the carbon gain capacity of glycophytes (Ball, 2002). For example, mangrove structural development and coverage in mixed mangrove–freshwater swamp formations at the Amazon river mouth is reduced owing to the strong influence of freshwater discharge, in contrast to well-developed stands (e.g., AGB > 200 Mg/ha) on the north side of the Amazon delta, where tidal forcing prevails over riverine discharge (Rovai et al., 2016; Schaeffer-Novelli et al., 1990).

Mangrove AGB in lagoons (type IV) was intermediate relative to river- and tide-dominated and arheic coastlines, reflecting the relative contribution of tidal forcing in this type of coastal environmental setting (Woodroffe et al., 2016). AGB was lowest in arheic coastal environmental settings in both biogeographical regions (e.g., Baja California in AEP, Persian Gulf and south-western Australia in IWP), reflecting osmotic stress caused by limited freshwater supply (Adame et al., 2020). In addition to tidal amplitude (Rovai et al., 2016), we found that tidal cycle duration is a significant predictor of mangrove AGB variation globally. Longer tidal cycles allow for higher loading of nutrient-rich particles, increasing soil fertility (Adame et al., 2010). Moreover, increased tidal flushing promotes vigorous mixing of tidal

waters, and oxygenation and removal of phytotoxins (e.g., sulfide) from stagnant waterlogged soils (Cameron et al., 2019). Although plant productivity–inundation functions (Cahoon et al., 2020) are expected to scale up across hierarchical organization levels, it is remarkable that global patterns in AGB emerge as a response to inundation time at the scale of our study, given the large variability in AGB values at any given latitudinal zone.

Aboveground biomass in carbonate mangroves was similar to river- and tide-dominated systems, highlighting the importance of these coastal settings as significant hotspots for carbon storage in AGB in addition to high SOC densities (Rovai et al., 2018). For example, tall, well-developed (e.g., basal area 20–40 m^2/ha; height > 15 m) mangrove forests can develop on carbonate settings, particularly where stochastic processes, such as hurricanes, promote episodic nutrient (i.e., Ca-bound P) loading, such as in south-western Florida Coastal Everglades (Castañeda-Moya et al., 2020; Chen & Twilley, 1999). Likewise, tall mangrove forests develop around "cenotes" (natural sinkholes), which provide a surface connection to subterranean nutrient-rich groundwater, as seen in the carbonate Yucatán peninsula (Adame et al., 2013). In addition, mangroves colonizing Holocene reef tops surrounding high oceanic islands with high precipitation (> 3 m/year) can receive considerable phosphorus input from weathering of phosphate rock beds (Fosberg, 1957) or via phreatic groundwater from geothermal endo-upwelling (Rougerie et al., 1997), allowing for higher forest structural development, such as in Micronesia (Ewel et al., 2003) and, possibly, in other relict oceanic mangrove stands with a high degree of structural development (Woodroffe, 1988).

Our study shows that tropical cyclones do not control the variability of mangrove AGB globally, as previously assumed from a relationship between mangrove canopy height and cyclone landfall frequency (Simard et al., 2019). In the present study, we tested this hypothesis directly with AGB estimates, rather than canopy height. Tropical cyclones fertilize mangroves, stimulating ecosystem productivity and recovery post-disturbance (Castañeda-Moya et al., 2020; Lovelock et al., 2011), which results in overall higher biomass relative to pre-storm conditions owing to increases in stand basal area and stem density (Imbert, 2018). This positive feedback can also generate inconsistencies in plot-level allometric relationships (e.g., broken crowns creating relatively shorter trees, but with large diameter). Moreover, cyclones shift proportional allocation from AGB to dead standing and downed necromass (i.e., coarse wood debris), which are crucial carbon pools and important pathways for remineralization in mangrove areas affected by cyclones (Krauss & Osland, 2020). Tropical cyclones, however, can also convert mangroves to mudflats or ghost forests when mechanisms that control sediment surface elevation (e.g., loss of root productivity) and depositional patterns (e.g., altered hydrological connectivity) are severely disrupted (Krauss & Osland, 2020; Osland et al., 2020).

Most importantly, the direct influence of tropical cyclones on mangrove forest structure and function is rather localized, and not a global phenomenon occurring over the totality of mangrove area. We estimated that a maximum of 40% of the global mangrove area (Hamilton & Casey, 2016) could potentially overlap with the radius of maximum winds of tropical cyclones (for details, see Supporting Information and Figure S6). This, however, is likely to be an overestimate, because wind speed decreases exponentially with increasing distance from the track of storms, as does its influence over mangrove forest structure (Doyle et al., 2009). Thus, although tropical cyclones might constrain canopy heights in regions subjected to this cyclical disturbance regime, the global variability in mangrove biomass appears to be related more closely to other global geophysical and climatic factors, as shown by our results.

4.3 | Ecosystem-level carbon stocks in mangroves across broad global geographical gradients

Predicted carbon stocks in biomass are consistent with the variability of observed AGB values, decreasing from river- and tide-dominated to carbonate and arheic coastal environmental settings. The SOC density was lower in river- and tide-dominated systems relative to lagoon and carbonate coastal environmental settings, although this gradient was not as marked when compared with observed values, probably reflecting higher environmental variability than captured in previous datasets (Rovai et al., 2018; Twilley et al., 2018). Consistent with earlier findings (Atwood et al., 2017), carbon stored in AGB and soils was poorly correlated ($R^2 = .016$, $p < .001$), possibly reflecting distinct functional mechanisms of biomass allocation across diverse coastal environmental settings. For example, although AGB can vary by orders of magnitude within the same coastal setting, SOC density has a much more uniform distribution across the landscape (Adame et al., 2013; Castañeda-Moya et al., 2013). In addition, much of the mangrove SOC comes from terrestrial and marine allochthonous sources, particularly in minerogenic river-dominated and macrotidal systems, which also influences this carbon pool (Cragg et al., 2020).

Our results suggest that biomass partitioning in mangrove communities across broad geographical gradients is explained by allometric scaling properties. Mechanisms structuring large-scale spatial patterns in mangrove forest structure and AGB are associated with meso-scale environmental drivers at the level of the coastal environmental setting. At this scale, mangrove forest structure and biomass apportioning reflect energy dissipation strategies in response to many ecological factors that regulate metabolic production, causing much of the variability in AGB within any coastal morphology, as captured in our data. From an evolutionary perspective, plant-dominated communities converged to a limited number of phenotypic expressions (or designs) as a result of optimization processes and trade-offs needed to ensure perpetuity (e.g., survival, growth, reproductive fitness) (Enquist & Niklas, 2001). This resulted in a number of biomass allocation patterns across variable environments (Enquist & Niklas, 2001). Mangrove forests evolved while confined to a much more limited number of coastal environments and latitudinal range relative to terrestrial forests (Ellison, 2002); nonetheless, it is intuitive to think they abide by the same fundamental trade-off patterns described for their terrestrial forested counterparts. In

mangroves, resource availability and plant resource-use efficiency vary conspicuously among coastal environmental settings, which determines how biomass is partitioned within individuals and across space, ranging across multiple spatial scales.

4.4 | Conclusions

This study advances our understanding of the spatial variability in mangrove forest structure and AGB at a global scale and provides new insights into key environmental drivers responsible for such variation. Our models are grounded on a systems ecology perspective, showing how mangrove AGB distribution is controlled by broad environmental drivers, rather than estimates based on other forest attributes (e.g., canopy height) or artificial proxies, such as latitude. In addition to bioclimatic drivers (e.g., precipitation, temperature), our results show that tidal amplitude and duration are important factors that control mangrove AGB globally. This finding is particularly relevant because mangroves and other types of coastal wetlands mostly develop in estuarine settings, where salinity levels, nutrient and sediment deposition, and hydroperiod (particularly, the duration of inundation) are largely regulated by tides.

Furthermore, this study reconciles views of the macroecology of wetlands and terrestrial forests. Remarkable similarities in stand structural complexity and tree mass–density relationships between biogeographical regions and among most coastal environmental settings show that resource allocation in mangrove ecosystems is independent of individual tree size and invariant to species composition or latitude. Mangrove wetlands closely follow a fractal-based scaling relationship that describes biomass allocation per unit area for several other terrestrial tree-dominated communities. Notably, different estimates across studies, attributable, in part, to the different allometric equations used, highlight the pressing need to use standardized frameworks to derive global carbon estimates in coastal wetlands, because carbon stocks result largely from biomass production and allocation. Our data show that the mass–density relationship can be used as a strong predictor of mangrove AGB, accounting for some of the stand stocking variability under the canopy that remote sensors are currently unable to capture. Understanding how mangrove forests are controlled by universal allometric rules can improve our ability to account for biomass apportioning within and across mangrove communities globally in response to broad geographical gradients. Lastly, this study provides an empirical basis and data that could support other macroecological investigations, such as habitat complexity for species distribution assessments, in addition to nature-based strategies for coastal resilience (e.g., protection against cyclonic-induced storm surges and wind–wave energy dissipation).

ACKNOWLEDGMENTS

The authors are thankful to all scientists and field crew who collected and processed the vast amount of data used in this paper. Louisiana Sea Grant College partially funded A.S.R. and R.R.T. The Coordenação de Aperfeiçoamento de Pesssoal de Nível Superior (CAPES) and the Conselho Nacional de Desenvolvimento Científico e Tecnológico (CNPq), through the Science without Borders and Post-doctoral Senior program, provided fellowships for A.S.R. (BEX1930/13-3), P.R.P. (BEX18379/12-5) and A.L.F. (BEX209666/13-7). Partial funding for E.C.-M. was provided by the National Science Foundation (NSF) through the Florida Coastal Everglades Long-Term Ecological Research Program (grant no. DEB-1832229). A.A. was supported by the USAID Indonesia Forest and Climate Supports (IFACS; contract no. AG-3187-C-13-0010). P.H.T. is thankful to the U.S. Forest Service International Programs (USFS/IP) for funding data collection. This is contribution number #1002 from the Southeast Environmental Research Center in the Institute of Environment at Florida International University.

CONFLICT OF INTEREST

The authors declare no conflict of interest.

AUTHOR CONTRIBUTIONS

A.S.R. conceived the study, collated data from the literature, performed statistical analyses and wrote the manuscript draft. A.S.R., P.R. and A.E.L.S. performed geospatial analyses. R.R.T., E.C.-M., D.A.F., C.C.T., J.J.B., S.D.S., S.R.M., P.R.P. and A.L.F assisted in gathering data from the literature and writing the manuscript draft. R.R.T., J.J.B., R.A.M., C.C.T., A.A., S.D.S., D.A.F., M.S., T.G.C., J.P., M.W.W., D.M., W.M., S.S. and P.H.T. contributed unpublished data. All authors reviewed and contributed to the final draft of the manuscript.

DATA AVAILABILITY STATEMENT

The dataset that supports the findings of this study is archived at https://doi.org/10.6084/m9.figshare.13570601

ORCID

Andre S. Rovai https://orcid.org/0000-0003-4117-2055
Robert R. Twilley https://orcid.org/0000-0002-6173-6033
Edward Castañeda-Moya https://orcid.org/0000-0001-7759-4351
Stephen R. Midway https://orcid.org/0000-0003-0162-1995
Daniel A. Friess https://orcid.org/0000-0002-3087-5233
Carl C. Trettin https://orcid.org/0000-0003-0279-7191
Jacob J. Bukoski https://orcid.org/0000-0002-2334-5023
Atticus E.L. Stovall https://orcid.org/0000-0001-9512-3318
Paulo R. Pagliosa https://orcid.org/0000-0003-0834-2534
Alessandra L. Fonseca https://orcid.org/0000-0001-7488-1611
Richard A. Mackenzie https://orcid.org/0000-0001-6799-6218
Aslan Aslan https://orcid.org/0000-0003-3362-4509
Sigit D. Sasmito https://orcid.org/0000-0001-7272-572X
Mériadec Sillanpää https://orcid.org/0000-0002-0013-4936
Thomas G. Cole https://orcid.org/0000-0002-8294-1108
Joko Purbopuspito https://orcid.org/0000-0002-4631-596X
Matthew W. Warren https://orcid.org/0000-0001-6021-4818
Daniel Murdiyarso https://orcid.org/0000-0001-5497-6293
Sahadev Sharma https://orcid.org/0000-0001-7602-7419
Pham Hong Tinh https://orcid.org/0000-0002-1293-253X
Pablo Riul https://orcid.org/0000-0003-4035-1975

REFERENCES

Adame, M. F., Kauffman, J. B., Medina, I., Gamboa, J. N., Torres, O., Caamal, J. P., Reza, M., & Herrera-Silveira, J. A. (2013). Carbon stocks of tropical coastal wetlands within the karstic landscape of the Mexican Caribbean. *PLoS One*, *8*, e56569. https://doi.org/10.1371/journal.pone.0056569

Adame, M. F., Neil, D., Wright, S. F., & Lovelock, C. E. (2010). Sedimentation within and among mangrove forests along a gradient of geomorphological settings. *Estuarine, Coastal and Shelf Science*, *86*, 21–30. https://doi.org/10.1016/j.ecss.2009.10.013

Adame, M. F., Reef, R., Santini, N. S., Najera, E., Turschwell, M. P., Hayes, M. A., Masque, P., & Lovelock, C. E. (2020). Mangroves in arid regions: Ecology, threats, and opportunities. *Estuarine, Coastal and Shelf Science*, 106796.

Analuddin, K., Suwa, R., & Hagihara, A. (2009). The self-thinning process in mangrove *Kandelia obovata* stands. *Journal of Plant Research*, *122*, 53–59. https://doi.org/10.1007/s10265-008-0190-8

Atwood, T. B., Connolly, R. M., Almahasheer, H., Carnell, P. E., Duarte, C. M., Ewers Lewis, C. J., Irigoien, X., Kelleway, J. J., Lavery, P. S., Macreadie, P. I., Serrano, O., Sanders, C. J., Santos, I., Steven, A. D. L., & Lovelock, C. E. (2017). Global patterns in mangrove soil carbon stocks and losses. *Nature Climate Change*, *7*, 523–528. https://doi.org/10.1038/nclimate3326

Ball, M. C. (2002). Interactive effects of salinity and irradiance on growth: Implications for mangrove forest structure along salinity gradients. *Trees*, *16*, 126–139. https://doi.org/10.1007/s00468-002-0169-3

Bukoski, J. J., Elwin, A., MacKenzie, R. A., Sharma, S., Purbopuspito, J., Kopania, B., Apwong, M., Poolsiri, R., & Potts, M. D. (2020). The role of predictive model data in designing mangrove forest carbon programs. *Environmental Research Letters*, *15*, 084019. https://doi.org/10.1088/1748-9326/ab7e4e

Cahoon, D. R., McKee, K. L., & Morris, J. T. (2020). How plants influence resilience of salt marsh and mangrove wetlands to sea-level rise. *Estuaries and Coasts*, https://doi.org/10.1007/s12237-020-00834-w

Cameron, C., Hutley, L. B., & Friess, D. A. (2019). Estimating the full greenhouse gas emissions offset potential and profile between rehabilitating and established mangroves. *Science of the Total Environment*, *665*, 419–431. https://doi.org/10.1016/j.scitotenv.2019.02.104

Castañeda-Moya, E., Rivera-Monroy, V. H., Chambers, R. M., Zhao, X., Lamb-Wotton, L., Gorsky, A., Gaiser, E. E., Troxler, T. G., Kominoski, J. S., & Hiatt, M. (2020), Hurricanes fertilize mangrove forests in the Gulf of Mexico (Florida Everglades, USA). *Proceedings of the National Academy of Sciences USA*, *117*, 4831–4841.

Castañeda-Moya, E., Twilley, R. R., & Rivera-Monroy, V. H. (2013). Allocation of biomass and net primary productivity of mangrove forests along environmental gradients in the Florida Coastal Everglades, USA. *Forest Ecology and Management*, *307*, 226–241. https://doi.org/10.1016/j.foreco.2013.07.011

Chen, R., & Twilley, R. R. (1999). Patterns of mangrove forest structure and soil nutrient dynamics along the Shark River Estuary, Florida. *Estuaries*, *22*, 955–970. https://doi.org/10.2307/1353075

Cormier, N., Twilley, R. R., Ewel, K. C., & Krauss, K. W. (2015). Fine root productivity varies along nitrogen and phosphorus gradients in high-rainfall mangrove forests of Micronesia. *Hydrobiologia*, *750*, 69–87. https://doi.org/10.1007/s10750-015-2178-4

Cragg, S. M., Friess, D. A., Gillis, L. G., Trevathan-Tackett, S. M., Terrett, O. M., Watts, J. E. M., Distel, D. L., & Dupree, P. (2020). Vascular plants are globally significant contributors to marine carbon fluxes and sinks. *Annual Review of Marine Science*, *12*, 469–497. https://doi.org/10.1146/annurev-marine-010318-095333

Doyle, T. W., Krauss, K. W., & Wells, C. J. (2009). Landscape analysis and pattern of hurricane impact and circulation on mangrove forests of the Everglades. *Wetlands*, *29*, 44–53. https://doi.org/10.1672/07-233.1

Duke, N. C., Shing, V. H. R., Lee, Y., Kristensen, E., & Twilley, R. R. (2017). Mangrove floristics and biogeography revisited: Further deductions from biodiversity hot spots, ancestral discontinuities, and common evolutionary processes. In V. H. Rivera-Monroy, S. Y. Lee, E. Kristensen, & R. R. Twilley (Eds.), *Mangrove ecosystems: A global biogeographic perspective* (pp. 17–53). Springer Nature.

Dürr, H. H., Laruelle, G. G., van Kempen, C. M., Slomp, C. P., Meybeck, M., & Middelkoop, H. (2011). Worldwide typology of nearshore coastal systems: Defining the estuarine filter of river inputs to the oceans. *Estuaries and Coasts*, *34*, 441–458. https://doi.org/10.1007/s12237-011-9381-y

Ellison, A. M. (2002). Macroecology of mangroves: Large-scale patterns and processes in tropical coastal forests. *Trees*, *16*, 181–194. https://doi.org/10.1007/s00468-001-0133-7

Enquist, B. J., Brown, J. H., & West, G. B. (1998). Allometric scaling of plant energetics and population density. *Nature*, *395*, 163–165. https://doi.org/10.1038/25977

Enquist, B. J., & Niklas, K. J. (2001). Invariant scaling relations across tree-dominated communities. *Nature*, *410*, 655–741. https://doi.org/10.1038/35070500

Ewel, K. C., Hauff, R. D., & Cole, T. G. (2003). Analyzing mangrove forest structure and species distribution on a Pacific island. *Phytocoenologia*, *33*, 251–266. https://doi.org/10.1127/0340-269X/2003/0033-0251

Ferreira, J., Lennox, G. D., Gardner, T. A., Thomson, J. R., Berenguer, E., Lees, A. C., Mac Nally, R., Aragão, L. E. O. C., Ferraz, S. F. B., Louzada, J., Moura, N. G., Oliveira, V. H. F., Pardini, R., Solar, R. R. C., Vieira, I. C. G., & Barlow, J. (2018). Carbon-focused conservation may fail to protect the most biodiverse tropical forests. *Nature Climate Change*, *8*, 744–749. https://doi.org/10.1038/s41558-018-0225-7

Fosberg, F. R. (1957). Description and occurrence of atoll phosphate rock in Micronesia. *American Journal of Science*, *255*, 584–592. https://doi.org/10.2475/ajs.255.8.584

Giri, C., Ochieng, E., Tieszen, L. L., Zhu, Z., Singh, A., Loveland, T., Masek, J., & Duke, N. (2011). Status and distribution of mangrove forests of the world using earth observation satellite data. *Global Ecology and Biogeography*, *20*, 154–159.

Hamilton, S. E., & Casey, D. (2016). Creation of a high spatio-temporal resolution global database of continuous mangrove forest cover for the 21st century (CGMFC-21). *Global Ecology and Biogeography*, *25*, 729–738. https://doi.org/10.1111/geb.12449

Hamilton, S. E., & Friess, D. A. (2018). Global carbon stocks and potential emissions due to mangrove deforestation from 2000 to 2012. *Nature Climate Change*, *8*, 240–244. https://doi.org/10.1038/s41558-018-0090-4

Hijmans, R. J. (2020). raster: Geographic data analysis and modeling. R package. 249. https://CRAN.R-project.org/package=raster

Holdridge, L., Grenke, W. C., Hatheway, W. H., Liang, T., & Tosi, J. Jr. (1971). *Forest environments in tropical life zones: A pilot study*. Pergamon Press.

Hutchison, J., Manica, A., Swetnam, R., Balmford, A., & Spalding, M. (2014). Predicting global patterns in mangrove forest biomass. *Conservation Letters*, *7*, 233–240. https://doi.org/10.1111/conl.12060

Imbert, D. (2018). Hurricane disturbance and forest dynamics in east Caribbean mangroves. *Ecosphere*, *9*, e02231. https://doi.org/10.1002/ecs2.2231

Kamara, M., & Kamruzzaman, M. (2020). Self-thinning process, dynamics of aboveground biomass, and stand structure in overcrowded mangrove *Kandelia obovata* stand. *Regional Studies in Marine Science*, *38*, 101375. https://doi.org/10.1016/j.rsma.2020.101375

Kauffman, J. B., Adame, M. F., Arifanti, V. B., Schile-Beers, L. M., Bernardino, A. F., Bhomia, R. K., Donato, D. C., Feller, I. C., Ferreira, T. O., Jesus Garcia, M. D. C., MacKenzie, R. A., Megonigal, J. P., Murdiyarso, D., Simpson, L., & Hernández Trejo, H. (2020). Total ecosystem carbon stocks of mangroves across broad global environmental and physical gradients. *Ecological Monographs*, *90*, e01405. https://doi.org/10.1002/ecm.1405

Komiyama, A., Ong, J. E., & Poungparn, S. (2008). Allometry, biomass, and productivity of mangrove forests: A review. *Aquatic Botany*, *89*, 128–137. https://doi.org/10.1016/j.aquabot.2007.12.006

Krauss, K. W., & Ball, M. C. (2013). On the halophytic nature of mangroves. *Trees*, *27*, 7–11. https://doi.org/10.1007/s00468-012-0767-7

Krauss, K. W., & Osland, M. J. (2020). Tropical cyclones and the organization of mangrove forests: A review. *Annals of Botany*, *125*, 213–234. https://doi.org/10.1093/aob/mcz161

Liaw, A., & Wiener, M. (2002). Classification and regression by randomForest. *R News*, *2*, 18–22.

Lovelock, C. E., Feller, I. C., Adame, M. F., Reef, R., Penrose, H. M., Wei, L., & Ball, M. C. (2011). Intense storms and the delivery of materials that relieve nutrient limitations in mangroves of an arid zone estuary. *Functional Plant Biology*, *38*, 514–522. https://doi.org/10.1071/FP11027

Osland, M. J., Feher, L. C., Anderson, G. H., Vervaeke, W. C., Krauss, K. W., Whelan, K. R. T., Balentine, K. M., Tiling-Range, G., Smith, T. J., 3rd., & Cahoon, D. R. (2020). A Tropical cyclone-induced ccological regime shift: Mangrove forest conversion to mudflat in Everglades National Park (Florida, USA). *Wetlands*, *40*, 1445–1458.

Osland, M. J., Feher, L. C., Griffith, K. T., Cavanaugh, K. C., Enwright, N. M., Day, R. H., Stagg, C. L., Krauss, K. W., Howard, R. J., Grace, J. B., & Rogers, K. (2017). Climatic controls on the global distribution, abundance, and species richness of mangrove forests. *Ecological Monographs*, *87*, 341–359. https://doi.org/10.1002/ecm.1248

R Core Team. (2020). *R: A language and environment for statistical computing*. R Foundation for Statistical Computing. https://www.R-project.org/

Rougerie, F., Jehl, C., & Trichet, J. (1997). Phosphorus pathways in atolls: Interstitial nutrient pool, cyanobacterial accumulation and Carbonate-Fluoro-Apatite (CFA) precipitation. *Marine Geology*, *139*, 201–217. https://doi.org/10.1016/S0025-3227(96)00111-9

Rovai, A. S., Coelho-Jr, C., de Almeida, R., Cunha-Lignon, M., Menghini, R. P., Twilley, R. R., Cintrón-Molero, G., & Schaeffer-Novelli, Y. (2021). Ecosystem-level carbon stocks and sequestration rates in mangroves in the Cananéia-Iguape lagoon estuarine system, southeastern Brazil. *Forest Ecology and Management*, *479*, 118553. https://doi.org/10.1016/j.foreco.2020.118553

Rovai, A. S., Riul, P., Twilley, R. R., Castañeda-Moya, E., Rivera-Monroy, V. H., Williams, A. A., Simard, M., Cifuentes-Jara, M., Lewis, R. R., Crooks, S., Horta, P. A., Schaeffer-Novelli, Y., Cintrón, G., Pozo-Cajas, M., & Pagliosa, P. R. (2016). Scaling mangrove aboveground biomass from site-level to continental-scale. *Global Ecology and Biogeography*, *25*, 286–298. https://doi.org/10.1111/geb.12409

Rovai, A. S., Twilley, R. R., Castañeda-Moya, E., Riul, P., Cifuentes-Jara, M., Manrow-Villalobos, M., Horta, P. A., Simonassi, J. C., Fonseca, A. L., & Pagliosa, P. R. (2018). Global controls on carbon storage in mangrove soils. *Nature Climate Change*, *8*, 534–538. https://doi.org/10.1038/s41558-018-0162-5.

Schaeffer-Novelli, Y., Cintrón-Molero, G., Adaime, R. R., & de Camargo, T. M. (1990). Variability of mangrove ecosystems along the Brazilian coast. *Estuaries*, *13*, 204–218. https://doi.org/10.2307/1351590

Simard, M., Fatoyinbo, L., Smetanka, C., Rivera-Monroy, V. H., Castañeda-Moya, E., Thomas, N., & Van der Stocken, T. (2019). Mangrove canopy height globally related to precipitation, temperature and cyclone frequency. *Nature Geoscience*, *12*, 40–45. https://doi.org/10.1038/s41561-018-0279-1

Spalding, M., Kainuma, M., & Collins, L. (2010). *World atlas of mangroves*. Earthscan.

Tang, W., Zheng, M., Zhao, X., Shi, J., Yang, J., & Trettin, C. C. (2018). Big geospatial data analytics for global mangrove biomass and carbon estimation. *Sustainability*, *10*, 472. https://doi.org/10.3390/su10020472

Twilley, R., Chen, R., & Hargis, T. (1992). Carbon sinks in mangroves and their implications to carbon budget of tropical coastal ecosystems. *Water, Air and Soil Pollution*, *64*, 265–288. https://doi.org/10.1007/BF00477106

Twilley, R. R., Rovai, A. S., & Riul, P. (2018). Coastal morphology explains global blue carbon distributions. *Frontiers in Ecology and the Environment*, *16*, 503–508. https://doi.org/10.1002/fee.1937

White, E. P., Ernest, S. K. M., Kerkhoff, A. J., & Enquist, B. J. (2007). Relationships between body size and abundance in ecology. *Trends in Ecology and Evolution*, *22*, 323–330. https://doi.org/10.1016/j.tree.2007.03.007

Woodroffe, C. D. (1988). Relict mangrove stand on last interglacial terrace, Christmas Island, Indian Ocean. *Journal of Tropical Ecology*, *4*, 1–17. https://doi.org/10.1017/S0266467400002431

Woodroffe, C. D., Rogers, K., McKee, K. L., Lovelock, C. E., Mendelssohn, I. A., & Saintilan, N. (2016). Mangrove sedimentation and response to relative sea-level rise. *Annual Review of Marine Science*, *8*, 243–266. https://doi.org/10.1146/annurev-marine-122414-034025

WRI/IIED. (1986). *World resources 1986*. Basic Books, Inc.

BIOSKETCH

We are a team of coastal wetland scientists with international and interdisciplinary expertise on mangrove ecology, macroecology, biogeochemistry and forestry. We are interested in developing tools and integrating methods that improve current global mangrove carbon stock estimates and that help to advance conceptual and empirical questions of broad interest across fields such as macroecology, global biogeochemistry, biogeography, climate change and conservation biology.

SUPPORTING INFORMATION

Additional supporting information may be found online in the Supporting Information section.

How to cite this article: Rovai AS, Twilley RR, Castañeda-Moya E, et al. Macroecological patterns of forest structure and allometric scaling in mangrove forests. *Global Ecol Biogeogr.* 2021;30:1000–1013. https://doi.org/10.1111/geb.13268